Polymorphs, Solvatomorphs, Hydrate and Perhydrate of Dabrafenib

Sunil K. Rai,*[a,c] Anilkumar Gunnam,[b] Gregory J. O. Beran,[d] James A. Kaduk,[e] and Ashwini K. Nangia*[b,c]

[a] Department of Chemistry, Faculty of Science, University of Lucknow, Lucknow, Uttar Pradesh 226007, India
[b] School of Chemistry, University of Hyderabad, Prof. C. R. Rao Road, Gachibowli, Central University P.O., Hyderabad 500 046, India
[c] Division of Organic Chemistry, CSIR − National Chemical Laboratory, Dr. Homi Bhabha Road, Pune 411008, India
[d] Department of Chemistry, University of California Riverside, Riverside CA 92521, USA.
[e] Illinois Institute of Technology, 3101 S. Dearborn St., Chicago, Illinois 60616, USA and North Central College, 131 S. Loomis St., Naperville, Illinois 60540, USA

ABSTRACT: Crystal form screen of the anticancer drug Dabrafenib (DBF) was performed using a wide range of non-polar aprotic, polar aprotic and polar protic solvents. Extensive crystallization in these solvent systems produced three crystal forms (I, II and III) of the drug, a monohydrate, an isomorphous peroxo solvate, and eight different solvates with ethyl acetate, dichloromethane, chloroform, carbon tetrachloride, 1,1,2,2-tetrachloroethane, tetrachloroethylene, benzene, and anisole of DBF. Surprisingly no solvates were crystallized with alcohol solvents attempted. The novel crystalline forms were characterized by single-crystal X-ray diffraction (SC-XRD) or Structure Solution from Powder Data (SSPD). The neutral drug derived from the mesylate salt of DBF by neutralization (form Ia) and the crystallized form I exhibited almost similar powder X-ray diffraction (PXRD) line pattern but their differential scanning calorimetry (DSC) thermograms comparison showed significant differences. Thus, the structure of microcrystalline powder form Ia was solved from SDPD reflections showed the same molecular packing but conformational strain compared to form I (structure by SC-XRD). The relative stability of the drug polymorphs was calculated using dispersion-corrected density functional theory with an intramolecular conformationall energy correction. The calculations suggest that form II is the most stable polymorph and form III, form I and form Ia are progressively less stable. Residual water content analysis of the isomorphous peroxosolvate showed that it is a mixed hydrate/peroxosolvate with ~9.5% water occupancy quantified by ^{31}P NMR analysis of the peroxosolvate content using triphenylphosphine oxide. The supramolecular analysis and molecular packing of DBF crystal forms suggests that the molecule has a propensity to form solvates with aprotic solvents and more specifically with chlorohydrocarbons. With its high molecular flexibility, a prolific solvate potential and drug polymorphism, the present work opens opportunity for further solid form landscape study of the popular anticancer drug Dabrafenib.

1. Introduction

Solid form screening and selection of the optimal active pharmaceutical ingredient (API) formulation during process development is a crucial step in the pharmaceutical industry.[1-3] Polymorphs and solvatomorphs (including hydrates) are the general outcome of solid crystal form exploration and play a vital role in drug discovery and pharmaceutical development

because of the unique physicochemical properties of the desired crystalline form, such as color, melting point, solubility, stability, bulk density, flow properties and bioavailability.[4-8] Generally, the most stable crystal form at ambient temperature is preferred in the drug formulation. Therefore, solid forms of APIs are screened through crystallization using a number of different solvents at ambient conditions, along with crystallization at high pressure and through sublimation or from the melt is also employed to widen the search.[9-15] In addition, self-assembled monolayers (SAMs) and confinement in media are used to induce nucleation and control polymorphism.[16-18] These and other modern techniques are reported to solve novel crystal structures and achieve records in high number of polymorphs discovery.[19-23] Crystallization using solvents is preferred for an initial screening to check the API's propensity to form solvates and also to understand the crystallization system. In previous extensive studies, solvent crystallization have afforded (i) over a hundred solvated forms of sulfathiazole along with 5 neat forms,[4] (ii) 12 polymorphs with 9 solved structures of aripiprazole,[24] (iii) 9 polymorphs of flufenamic acid,[19] (iv) 60+ solvated forms of olanzapine with 6 neat forms,[25] (v) 70+ polymorphs and 5 neat forms of axitinib,[5] and (vi) 50+ polymorphs with 10 neat forms of galunisertib.[20] The record holder ROY with the highest number of solved crystal structures has twelve polymorphs, with five being observed during melt crystallization and cross-nucleation.[22,25,26] The above polymorphic systems were reported over several years and collective efforts from different research groups. The question always remains: how long one has to spend and how much effort invested to obtain all the polymorphs of a molecule and identify the thermodynamically most stable polymorph? Recent studies[20-23] suggest that we are getting closer to answer this question, crystal structure prediction (CSP) and structure determination from microcrystalline to amorphous materials using electron microscopy (EM) and solid-state nuclear magnetic resonance (ss-NMR) have significantly reduced the time required to identify the thermodynamically most stable polymorph.[27,28]

In this work, we have performed polymorph screening of dabrafenib (DBF), a small molecule inhibitor drug of $BRAF^{V600E}$ melanoma cells (Scheme 1a) to understand its structural landscape. According to McCrone,[29] the number of polymorphs of a compound is proportional to the time and energy spent in research on that compound. We carried out extensive experiments on polymorph screening using a wide range of solvents and conditions (Table S1 in Supporting Information). The free base solid of DBF was extracted from the mesylate salt by adding 5 N $NaHCO_3$ (named as form Ia).[30] To define the naming of polymorphs and solvates for this study, single crystal X-ray diffraction (SC-XRD) is reported for three drug polymorphs (form I, II and III), a monohydrate ($DBF{\cdot}H_2O$), an isostructural perhydrate ($DBF{\cdot}H_2O_2$), and eight solvates (with ethyl acetate = EA, dichloromethane = DCM, chloroform = TCM, carbon tetrachloride = CTC, 1,1,2,2-tetrachloroethane = TCE, tetrachloroethylene = PCE, benzene = BEN, and anisole = ANI) (Table S2 and S3 in Supporting Information). The structure of powder material (form Ia) obtained from the aqueous extract after neutralization and drying was determined by powder X-ray diffraction (SDPD) data and shows a similar conformation and packing resemblance with form I (Figure S1 and S2 in Supporting Information). This is the first structural report of DBF polymorphs to our knowledge. The possible polymorphs arise from conformational flexibility of the molecule and different supramolecular synthons.[31] DBF has four rotatable

bonds, out of which four (φ1-φ4) are potentially capable of conformational polymorphism (Scheme 1a). A fifth single bond C⟩S adjacent to φ1 will have restricted rotation due to 2,6-di-F-phenyl group. In terms of possible supramolecular synthons, DBF has two hydrogen bond donors (sulfonamide and aminopyrimidine hydrogen atoms) and five hydrogen bond acceptors (two oxygen atoms of sulfonamide, two nitrogen atoms of aminopyrimidine and one thiazole N), suggesting that there are several possibilities of homo and heterosynthons in its crystal structures (Scheme 1b-f).[32] These preliminary results hint that DBF could have the potential to become a high number of polymorphs and solvatomorphs drug molecule.

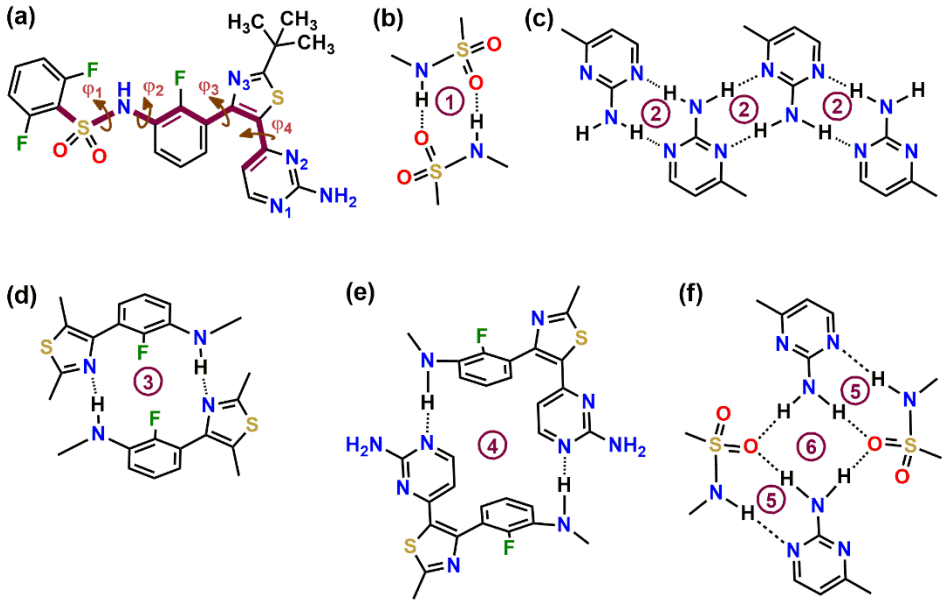

Scheme 1. (a) Chemical structure of DBF, and representation of dihedral angles φ_1, φ_2, φ_3 and φ_4 through bold grey colour bonds, and (b-f) represent some possible supramolecular synthons in the form of ring motif where 1, 2 and 5 are $R_2^2(8)$ graph sets, 3 = $R_2^2(14)$, 4 = $R_2^2(22)$, and 6 = $R_4^2(8)$.

2. Results and Discussion

2.1. Solid-Form Screen. All crystallization experiments were performed using form Ia sample of free DBF prepared in our lab. Crystallization of Ia from alcoholic solvents afforded form I exclusively, consistently from methanol and ethanol while isopropanol and n-butanol were not so reproducibly consistent. Continuing the crystallization from iso-butanol produced forms II and III concomitantly. After extensive screening of solvents, form II was crystallized from either isobutyl methyl ketone, and aromatic solvents such as toluene, xylene or chlorobenzene. Exclusive crystallization of form III was reproducible from isopropyl acetate. The almost similar PXRD pattern of form Ia and form I (Figure S1 in Supporting Information), indicated that they are the same crystal form, but their different DSC thermograms motivated us to determine the crystal structure of form Ia by powder diffraction structure solution, SDPD (Figure S2 in Supporting Information). A surprising and unexpected observation was the similar packing pattern and conformation of the molecule in both crystal structures, but with slight conformational adjustment in the molecular arrangement (see cif

files).[8] Such minor differences might arise because of the rapid reactive precipitation during neutralization of the mesylate salt to 1a.

2.2. Crystal structures of drug polymorphs. From a crystal engineering view point the analysis of supramolecular synthons and molecular conformations and crystal packing of different polymorphs offer a guide to understand the occurrence of polymorphism and also to predict further possibilities of new polymorphs. The hydrogen bond synthons in form I (space group $P\bar{1}$) are depicted in Figure 1, wherein a heterosynthon between sulfonamide and 2-aminopyrimidine occurs as the primary motif with graph set $R_2^2(8)$ (motif 5) and $R_4^2(8)$ (motif 6) ring.[33] The centrosymmetric arrangement of two DBF molecules results in dimer motif 5 and a larger ring $R_2^2(22)$ (motif 4) through one of the sulfone hydrogen atom and a pyrimidine ring nitrogen (N1) atom (homosynthon). In comparison, form II shows homosynthons 2 and 3 of $R_2^2(8)$, and $R_2^2(14)$graph set notation. Motif $R_2^2(8)$ is a centrosymmetric dimer of 2-aminopyrimidine rings, while $R_2^2(14)$ motif is constructed through sulfonamide group and thiazole ring (Figure 1b). The molecular packing in form III shows a homosynthon (motif 2) and a heterosynthon (motif 5) of graph set $R_2^2(8)$ (Figure 1c). Among the two ring nitrogen atoms of 2-aminopyrimidine ring the $R_2^2(8)$ ring in form I (motif 5) and form II (motif 2) are formed at N1 atom while N2 is free from strong hydrogen bonding in the crystal structures. In the case of form III, the heterosynthon motif 5 is constructed between 2-aminopyrimidine ring and sulfonamide group, where the hydrogen atom at sulfonamide group interacts with the N3 atom rather than with N1 (as observed in form I), but homosynthon motif 2 is formed at N1 (same as in form II). An intermolecular π···π stacking between terminal aryl rings in DBF polymorphs was also observed but only difference was in the orientation of aryl ring with respect to the molecular backbone (i.e., exo or endo orientation as shown in Scheme 1 in SI). Form I and II show an exo orientation of stacked terminal aryl rings, however in form III it is in endo orientation Because of the isosteric (similar volume) nature of hydrogen and fluorine atoms, and the role of fluorine interactions in the organic crystals, investigating the C–F···π interactions in DBF polymorphs is equally important as C–H···π interactions.[34-40] Therefore, quantitative intermolecular interactions were analyzed and shown in Figure 2.

The packing of DBF molecules and their interactions and synthons in the crystal structures of three polymorphs are different. Form II has the highest density and form III is a low-density polymorph (Table S2 in Supporting Information). The low density of form III is due to solvent assessable voids of ~1.2 Å probe radius (Figure 1g). In general, among several polymorphs of a flexible molecules, the structure has a more open conformation as the crystal density decreases.[41] However, there are several other factors that collectively determine the polymorph stability.[8,41] An overlay of three polymorphs around the central aryl ring (Figure 1h) shows a folded conformation of form II (ρ = 1.52 g cm^{-1}), a half-open conformation of form I (ρ = 1.49 g cm^{-1}), and an open conformation of form III (ρ = 1.42 g cm^{-1}).

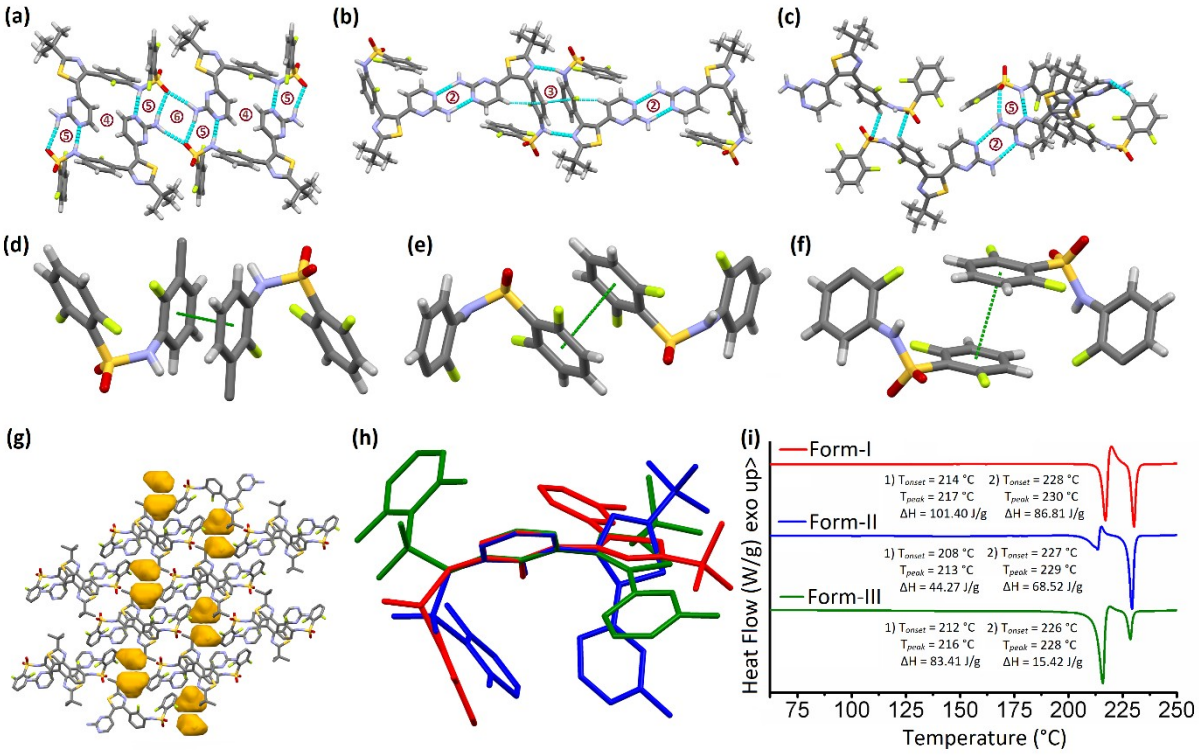

Figure 1. Selected interactions in DBF polymorphs (a) form I, (b) form II, (c) form III, (d) π···π stacking between central aryl rings in form II, (e) exo π···π stacking of terminal aryl rings in form I and II, (f) endo π···π stacking of terminal aryl rings in form III, (g) voids in the crystal packing of form III, (h) molecular structure overlay of form I (red), II (blue) and III (green) on central aryl ring, and (i) stack plot of DSC thermogram of form I (red), II (blue) and III (green).

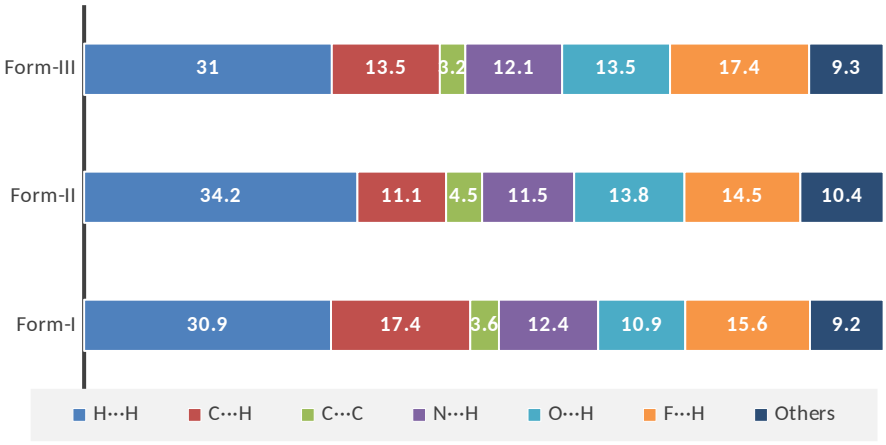

Figure 2. Percentage contribution of various intermolecular interactions in forms I, II and III. Calculations were done through CrystalExplorer 17.

2.3. Differential scanning calorimetry (DSC) of drug polymorphs. Thermal behavior of DBF polymorphs was examined by DSC. Form Ia show a single melting endotherm at ~215 °C (ΔH = 90.33 J/g) without any phase transition (Figure S4 in Supporting Information).

However, form I, II and III show a solid-solid phase transition between 210-220 °C and finally melt at ~230 °C (Figure 1i). It indicates that thermodynamically most stable polymorph (corresponds to ~230 °C) has yet to be crystallized. The polymorph corresponding to melting at ~230 °C can be named as form IV (melting onset 227 ± 1 °C) that may get crystallize in near future. From the crystallographic similarity, it was expected that form Ia and I should have the same a melting endotherm at ~215 °C, except say a slight variation in the heat of fusion (ΔH). Experimentally, form I shows an endotherm at ~215 °C (ΔH = 101.40 J/g) followed by immediate recrystallization (exotherm) to a new form which melts at ~230 °C (ΔH = 86.81 J/g). A similar pattern was observed for form II and III, but both endotherms show a significant difference with respect to their heat flow. The solid-solid phase transition endotherm in form II is observed at ~213 °C with comparatively lower ΔH (= 44.27 J/g) followed by immediate recrystallization to a new phase which melts at ~229 °C (ΔH = 68.52 J/g). This indicates that the first endotherm is a solid-solid phase transition rather than a melt and recrystallization process. Such transitions are observed due to slight relaxation of the intramolecular interactions and bonded molecules in the crystalline state. Notably, form II exists in a folded conformation with geometrical constraints. On the contrary, form III shows an endotherm at ~216 °C with a higher heat flow (ΔH = 83.41 J/g) compared to second endotherm (peak at ~228 °C, ΔH = 15.42 J/g). Since all solid forms are showing phase transformation upon heating (except form Ia), determining the actual experimental thermodynamic relationships among the polymorphs is challenging. The density rule of Burger and Ramberger would suggest that the polymorph with highest crystal density will be the most stable crystal form.[42] According to density rule, order of thermodynamic stability of DBF polymorphs is, from most to least stable, form II > form I > form III, though the density rule is at best a rough guide to stability, particularly for complex systems such as DBF.

2.4. Computational energy ranking of drug polymorphs. In contrast to the density rule correlation, periodic density functional theory (DFT) lattice energy calculations with dispersion-corrected B86bPBE-XDM function predict that form III is the most stable polymorph, having an energy 5.6 kJ/mol below that of form II. Upon geometry relaxation, forms I and Ia converge to nearly the same structure, with rmsd15 of 0.04 Å (Figure 3). This suggests that whatever differences exists between these crystal structures experimentally is not reproduced in the DFT calculations on the crystallographic unit cells. They also have very similar energies and lie 2.1-2.5 kJ/mol above form II. However, delocalization error inherent to generalized gradient approximation density functionals like B86bPBE predicts conformational energies poorly when the conformations differ in the extent of π conjugation.[43] In DBF, torsional angles φ3 and φ4 (Scheme 1) control the degree of conjugation between the aromatic rings. Most notably, the 77° angle of φ3 in form II disrupts nearly all conjugation between the two adjacent rings. In contrast, forms Ia, I, and III exhibit greater planarity/ conjugation between these rings, with φ3 angles of 42°, 42°, and 131°, respectively. This suggests that the DFT calculations probably artificially stabilize forms Ia, I, and III relative to form II.

To overcome this conformational energy issue, we performed a conformational energy correction[43] with domain-based local pair natural orbital coupled cluster theory (DLPNO-

CCSD(T)).[44] The correction subtracts the DFT conformational energy of the isolated (gas-phase) molecule(s) in their crystalline geometries with the corresponding DLPNO-CCSD(T) one as represented below in equation 1.

$$E_{crystal}^{corrected} = E_{crystal}^{DFT} + \sum_{i}^{monomers} \left(E_{monomer,i}^{DLPNO-CCSD(T)} - E_{monomer,i}^{DFT} \right) \qquad \text{(Equation 1)}$$

Eq 1 is evaluated by computing the crystal energy and the gas-phase monomer energies for each monomer in the unit cell, summing the terms together, and then computing the relative energy per molecule versus the most stable polymorph (form II). Because each crystal here contains only a single molecule in the asymmetric unit (Z'=1), the gas-phase calculations need to be run only once and the result can be multiplied by the number of symmetrically-equivalent monomers. This correction to the 0 K internal (electronic) energy of the crystal amounts to modelling the intramolecular conformational energy with DLPNO-CCSD(T), while the intermolecular interactions are described with DFT. The DLPNO approximation to CCSD(T) typically reproduces conventional CCSD(T) well albeit with a far lower computational cost that makes it feasible for large molecules like DBF. DLPNO-CCSD(T) does not suffer from delocalization error like the DFT model, so it should predict more reliably conformational energies. The conformational energy correction approach has proved useful in a number other crystal structures, including those of pharmaceuticals.[43,45,46]

Applying the conformational energy correction to the three DBF polymorphs destabilizes form III by 6.3 kJ/mol relative to form II, such that form II now lies 0.7 kJ/mol below form III (Figure 3). The conformational energy correction also destabilizes forms Ia and I by about 4.0 kJ/mol relative to form II, and they now lie 6.0 kJ/mol above the other two forms. In other words, the predicted stability ordering becomes form II ≈ form III > form I ≈ form Ia. Despite the nominal 0.7 kJ/mol predicted energy preference for form II over form III, accuracy limitations of the computational models and the focus on lattice energies instead of finite-temperature enthalpies or free energies prevent definitive ranking of these two polymorphs. It should be noted, however, that the similar energetics predicted for those two forms is consistent with the experimental observation that they grow concomitantly.

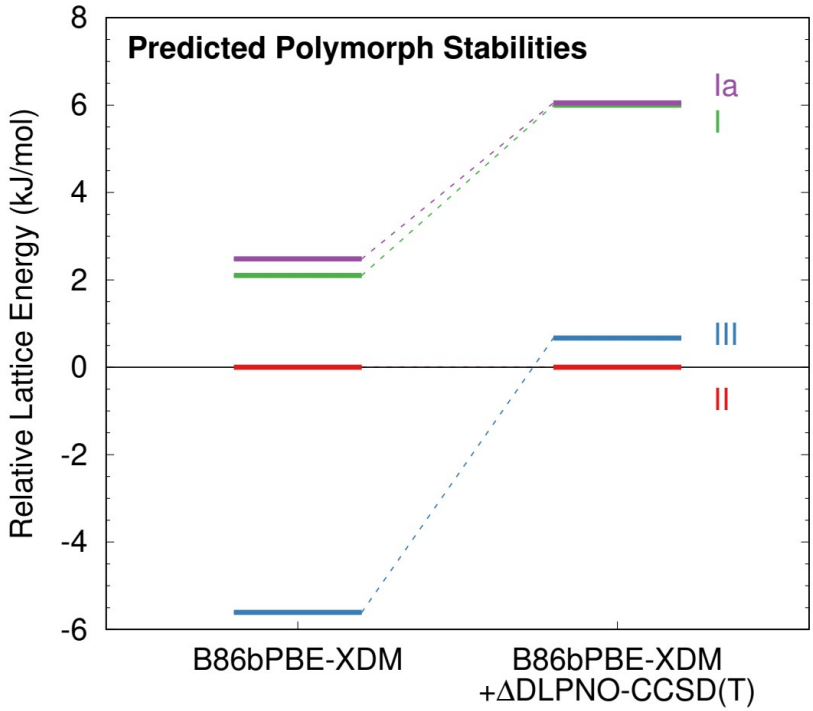

Figure 3. Calculated relative lattice energies of forms Ia, I, II and III using B86bPBE-XDM directly and after applying the DLPNO-CCSD(T) intramolecular conformational energy correction.

2.5. Crystal structures of hydrate and perhydrate. Due to ubiquitous nature of water, hydrate formation is a common phenomenon during polymorphs screening. Almost one-third of pharmaceutical solids are reported in their hydrate form.[47] Therefore, it is of paramount interest to discover possible hydrate forms in early drug screening to avoid any phase conversion during the development process and formulation.[3] DBF did not produce hydrates in routine crystallization experiments from several solvents. Subsequently, we checked the water activity on hydrate formation in different alcohols (i.e., methanol, ethanol, n-propanol and isopropanol). To our gratification, a monohydrate DBF·H_2O was crystallized in ~10% aqueous isopropanol as transparent shining crystals. We decided to further explore the concept of isostructural perhydrate formation because of the medicinal importance of drug-hydrogen peroxide cocrystals.[48] Crystallization of DBF in 9:1 ratio of isopropanol and hydrogen peroxide (30% v/v as available commercially) produced a perhydrate DBF·H_2O_2 which was found to be isomorphous with DBF·H_2O. Both crystal structures were solved in triclinic $P\bar{1}$ space group (Table S2 in Supporting Information). Hydrogen bond analysis showed that the water molecule forms two O–H···N, one N–H···O and one C–H···O interactions. Hydrogen peroxide forms two O–H···N, two N–H···O and one C–H···O interaction (Figure 4a and b). Overlapping of crystal packing of DBF·H_2O and DBF·H_2O_2 does not show significant differences, however, water molecule O resides exactly at the center of the peroxide O⟩O bond (Figure 4c). In such a case of isomorphous peroxo solvate, there is a chance of partial occupancy of H_2O/ H_2O_2 molecules at the same site. Therefore, there is a need to quantify the H_2O occupancy in mixed hydrate/peroxosolvate.[49] The X-ray diffraction data of DBF·H_2O_2 shows a residual peak of electron density (~0.4 e·$Å^{-3}$) at the

center of the O–O bond of H_2O_2 after anisotropic refinement of oxygen atoms. Although this is not a reliable method to quantify the water content but suggests that there may be residual water crystallized with DBF·H_2O_2 which occupy H_2O_2 crystal sites. Additionally, the DSC-TGA data of DBF·H_2O show that the water loss (~3.35%) occurred at ~150-160 °C with a solid-solid phase transition at ~140 °C (Figure S5a in Supporting Information). However, DBF·H_2O_2 (mixed hydrate/peroxo solvate) showed a broad endotherm between ~140-170 °C in DSC, and TGA showed continuous weight loss from ~130 °C to 225 °C (Figure S5b in Supporting Information). This suggests that the residual water in DBF·H_2O_2 escaped below 170 °C (i.e., <1% weight loss) and H_2O_2 evolution begins above 200 °C, and exudation was completed after the melt. These observations imply that H_2O_2 is tightly bound in the crystal lattice compared to H_2O molecules. Since the water content in DBF·H_2O_2 could not be calculated accurately by TGA, a chemical method was developed to measure it. An excess amount of triphenylphosphine (TPP) was reacted with a known amount of DBF·H_2O_2 (mixed hydrate/peroxo solvate) in anhydrous acetonitrile, such that H_2O_2 reacts with TPP to produce triphenylphosphine oxide (TPPO) (Equation S1 in Supporting Information). Subsequently, ^{31}P NMR spectrum was recorded, where integration of ^{31}P signals corresponding to the TPP (at up field) and the TPPO (at down field) showed the water content as ~9.50% (Figure S3 and calculations in Section 4 in Supporting Information).

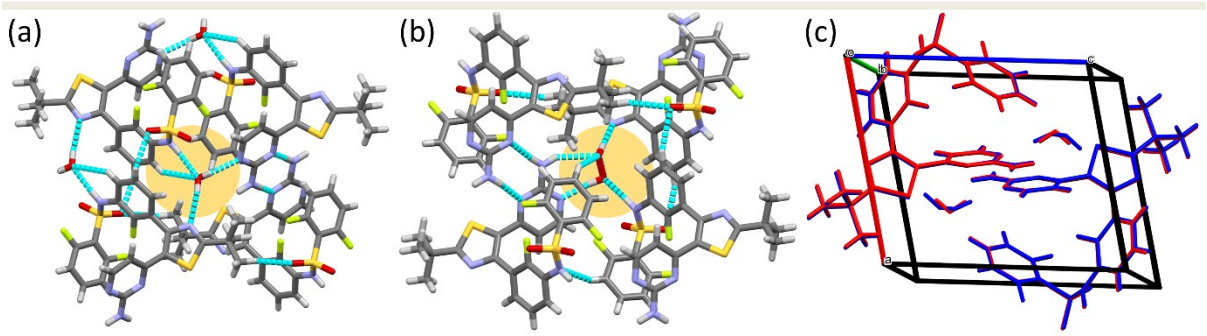

Figure 4. Representation of selected interactions in crystal structure of (a) DBF·H_2O, (b) DBF·H_2O_2, and (c) overlay of molecular packing in DBF·H_2O (red) and DBF·H_2O_2 (blue).

2.6. Crystal structures of solvatomorphs. To satisfy the regulatory authorities it is crucial to establish the crystal forms of an API through its solvates in a systematic polymorph screen. Therefore, along with a limited number of pharmaceutically acceptable solvents (mostly Class 3 solvents in Q3C guidance of ICH), one should also use pharmaceutically unacceptable solvents (i.e., Class 1 and 2 solvents in Q3C guidance of ICH and others) which might increase the probability of finding new polymorphs or solvates because of their specific behaviour with the solute molecules. During crystal form screening, isolation and characterization of stable solvates were recurrent, however unstable solvates were either desolvating immediately or converting to its lower stoichiometry of solvate. Several solvates are often overlooked during data collection because of their mere survival either at lower temperatures or in the mother liquor. Therefore, in the case of unstable solvates and the solvates obtained under very slow rate of crystallization, the exact experimental conditions determine the outcome of the crystallization of solvates. Among all solvates, DBF·DCM,

DBF·TCM, DBF·PCE, DBF·BEN and DBF·ANI were directly crystallized with excess solvent present by slow evaporation technique. Except anisole all are low boiling in the aforesaid solvents, therefore, SC-XRD data was collected at 100 K and crystals were directly taken from the mother liquor just to avoid desolvation. In case of low boiling solvated crystals (i.e., DCM, TCM, PCE and BEN), desolvation was observed through unaided eye because of their transparency loss within a few days when kept off the mother liquor under ambient conditions, and thus solid phase transformation is obvious. However, DBF·ANI crystals were stable enough under the same conditions. Our effort was to crystallize DBF not only in single solvents but also in mixtures of solvents, solvents with additives (in stoichiometric and nonstoichiometric ratios of DBF) and by varying the pH using weak acids and bases. Fortunately, crystal form of DBF·EA was isolated through a very slow crystallization of ethyl acetate solution (evaporation over 20-30 days; whereas at faster rate of crystallization under ambient condition the product was form I) whereas petroleum ether was used as diffusing solvent in a sealed glass vial. DBF·CTC was isolated from a mixture of carbon tetrachloride (CTC) and isobutyl alcohol (because of insolubility of DBF in CTC, isobutyl alcohol was used as crystallizing solvent and CTC was added ~10%). Crystallization of DBF in TCE produced form I while DBF·TCE was isolated during cocrystallizaion of 1,4-difluorobenzene and DBF in 1:1 ratio in TCE. Here, DBF·TCE is an outcome of screening of fluorobenzenes as a solvate/cocrystal former, the motivation of cocrystallization of fluorobenzenes was collectively obtained from (i) DBF·BEN, where structural similarity of fluorobenzenes and benzene is because of isosteric nature of hydrogen and fluorine atoms, and (ii) crystallization of DBF·H_2O, DBF·H_2O_2 and DBF·CTC, which indicated that even presence of a small fraction of a solvent (at least in a stoichiometry) in the mixture can be cocrystalized with DBF. Crystallization of DBF·TCE is a subject of further research to know whether it is a template-induced nucleation or controlled by nucleation kinetics.

The analysis of molecular conformation, supramolecular synthons and arrangement of solvent molecules in the crystal structures of solvatomorphs could lead to the isolation of novel desolvated solid forms. DBF·EA was crystallized in monoclinic crystal system of space group *C*2/*c*. Solvent molecules formed channels (Figure 5a, b) and are stabilized by a few weak C–H···O, C–H···F and C–H···π interactions. However, there are no polar interactions among EA molecules in the solvent channel but hydrophobic interactions between terminal methyl groups are present. In case of DBF·DCM and DBF·TCM, which crystallized in space group $P2_1/c$ and $P\bar{1}$, solvent molecules are well separated and reside in the solvent voids. As shown in Figure 5c and 5d, DCM molecules in the crystal lattice of DBF·DCM are stabilized by weak interactions. However, TCM molecules in the crystal lattice of DBF·TCM are better stabilized by C–Cl···π interactions (Figure 5e-g). DBF·CTC crystallized in space group $P\bar{1}$, with one DBF molecule and three symmetrically independent CTC molecules, among them one molecule shows thermal disorder of chlorine atoms. Molecular packing shows that two CTC molecules are occupied in the solvent channel where the disordered molecule is at the center of the channel, while another one occupies the fissure region and a third is trapped in the inter-channel space (Figure 5h, i). CTC molecules in the crystal lattice of DBF·CTC are devoid of any polar interactions but poorly stabilized by C–Cl···π interactions (Table S4 in Supporting Information). Consequently, DBF·CTC lose its transparency within 1-2 hours

after removal from the mother liquor perhaps due to escaping of very loosely trapped CTC in the solvent channel which converts to the lower stoichiometry of the solvate. DBF·TCE and DBF·PCE both crystallized in space group $P\bar{1}$. Interestingly, molecular arrangement in the crystal packing of both solvates is same except slight variation in the strength of synthon interactions and cell parameters (Figure 5j-o). Further, in both cases, asymmetric unit possess one DBF molecule and two symmetrically independent solvent molecules. In DBF·TCE both solvent molecules are thermally disordered, however, in DBF·PCE only one molecule is disordered. Although, solvent molecules in the crystal lattice are not directly connected with each other through a non-covalent interaction, yet they are forming solvent channels. TCE molecules in solvent channels are stabilized by C–H···Cl interactions, however, PCE molecules are exclusively stabilized by C–Cl···π interactions (Table S4 in Supporting Information). Desolvation was observed in both the solvates when kept outside the mother liquor for 5-6 hours under ambient condition (at 25-30 °C). DBF·BEN crystallized in space group $P\bar{1}$ with two DBF molecules and four BEN molecules in the asymmetric unit. Molecular packing of DBF·BEN along the *b*-axis is shown in Figure 5p, where BEN molecules are trapped in the crystal voids. However, along a particular orientation of the packing, it shows a channel (Figure 5q) where all four BEN molecules are accommodated. The orientation of the BEN molecules in channel is devoid of C–H···π and π···π interactions but assisted only by van der Waals interactions. Like previous channel solvates, DBF·BEN also lose their transparency in 1-2 days after removal from the mother liquor. DBF·ANI crystallized in space group $P\bar{1}$ with four DBF molecules and five ANI molecules in the asymmetric unit. Molecular packing of DBF·ANI along *a*-axis is shown in Figure 5s, where ANI molecules occupy the solvent voids. In this case, ANI molecules are neither forming a channel nor showing any direct contact with each other except one C–H···π interaction between two ANI molecule. ANI molecules are stabilized through their unique C–H···π interactions with DBF molecules in the solvent voids. Because of desolvation and instability of most of the solvated forms, DSC and TGA was collected for selected solvates (Figure S6 in Supporting Information).

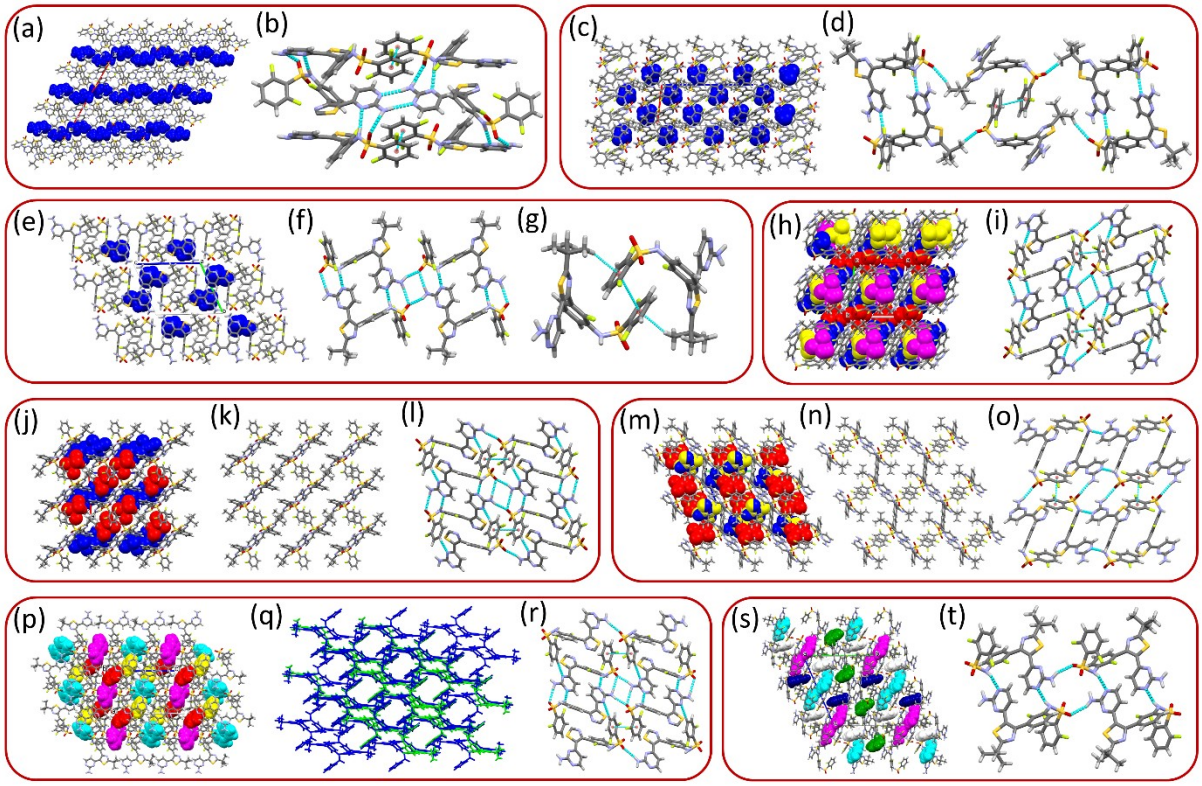

Figure 5. In the crystal packing of solvates, solvent molecules are shown in space fill model and colored by symmetry equivalence (a) packing of DBF·EA along *b*-axis, (b) supramolecular synthons in DBF·EA, (c) packing of DBF·DCM along *b*-axis, (d) supramolecular synthons in DBF·DCM, (e) packing of DBF·TCM along *a*-axis, (f & g) supramolecular synthons and aryl interactions in DBF·TCM, respectively, (h) packing of DBF·CTC along *c*-axis, (i) supramolecular synthons in DBF·CTC, (j) packing of DBF·TCE along *b*-axis, (k) packing framework of DBF·TCE after removal of solvent molecules which shows solvent channels, (l) supramolecular synthons in DBF·TCE, (m) packing of DBF·PCE along a-axis, (n) packing framework of DBF·PCE after removal of solvent molecules which shows solvent channels, (o) supramolecular synthons in DBF·PCE, (p) packing of DBF·BEN along *b*-axis, (q) packing framework of DBF·BEN after removal of solvent molecules which shows solvent channels, (r) supramolecular synthons in DBF·BEN, (s) packing of DBF·ANI along *a*-axis, and (t) supramolecular synthons in DBF·ANI. For clarity in the representation of supramolecular synthons, methyl groups are omitted.

3. Conclusions

Crystallization of DBF from a wide range of solvents produced three neat crystal forms (I, II and III), which were unambiguously characterized by single crystal X-ray diffraction. First-principles calculations using B86bPBE-XDM+ΔDLPNO-CCSD(T) suggest that form II is the most stable polymorph, though it is only marginally lower in lattice energy than that of form III (by ~0.7 kJ/mol). This small difference in lattice energy is consistent with the observed concomitant crystallization of polymorphs. Form I is ~6 kJ/mol higher in energy than form II. The water activity (above 10% v/v) in isopropanol plays significant role in crystallization of the monohydrate of DBF and the same condition produced isomorphous peroxosolvate by

using hydrogen peroxide as solvent (30% v/v in water). The crystallized peroxosolvate is a mixed hydrate/peroxosolvate with ~9.5% water occupancy. An extensive solvent screen produced eight solvates of DBF, namely with ethyl acetate, dichloromethane, chloroform, carbon tetrachloride, 1,1,2,2-tetrachloroethane, tetrachloroethylene, benzene, and anisole. The solvates were fully characterized by single crystal X-ray diffraction, but their crystal forms are highly unstable and desolvated to lower stoichiometry of solvent under ambient conditions. Therefore, thermal characterization of the same stoichiometry as observed in the crystal structure of solvates was difficult and required special attention. Supramolecular synthon analysis showed that the hydrogen bonds and intermolecular interactions in some higher solvates are different from those in pure drug polymorphs. It is possible that controlled desolvation and melt heating may yield new neat polymorphs of DBF. Our limited crystallization experiments but complete structural characterization suggests that DBF is a highly polymorphic drug molecule because of its flexible molecular structure with five rotatable dihedral bonds around the aromatic portion and could produce more crystal forms in future exploratory research.

4. Experimental procedures

4.1 General Methods. Mesylate salt of DBF was purchased from Swapan Roop Drugs & Pharmaceuticals (Aurangabad, Maharashtra, India). Neutral form of DBF was isolated from the aqueous extract of the salt by adding $NaHCO_3$ (5 M in water). Solvents used for crystallizations were purchased either from Sigma Aldrich or TCI Chemicals, and used without further purifications. All crystallizations were done at ambient temperature (between 20 to 30 °C) through solvent evaporations unless the specific conditions were not mentioned.

4.2. Single Crystal X-ray Crystallography. Single crystal X-ray diffraction data were collected on a Bruker SMART APEX II single crystal X-ray CCD diffractometer having graphite monochromatized (Mo-Kα, λ = 0.71073 Å) radiation at low temperature (100 K).[50] The X-ray generator was operated at 50 kV and 30 mA. The data reduction was performed using APEX-II Software. Intensities were corrected for absorption using SADABS,[50] and the structure was solved and refined using SHELX97.[51] All non-hydrogen atoms were refined anisotropically, and hydrogen atoms were geometrically fixed with thermal parameters equivalent to 1.2 times that of the atom to which they are bonded, except those H atoms which are involved in strong hydrogen bonding. Molecular diagrams for all compounds were prepared using ORTEP, and the packing diagrams were generated using Mercury version 3.10.[52] PLATON was used for the analysis of bond lengths, bond angles, and other geometrical parameters.[53] Crystallographic parameters of are summarized in Table S2, ORTEP diagrams in Table S3 and hydrogen bonds parameters are provided in Table S4. Crystal structures may be accessed at www.ccdc.cam.ac.uk/data_request/cif (CCDC nos. 2124747-2124759).

4.3. Thermal Analysis. Differential Scanning Calorimetry (DSC) analysis was performed on a Mettler Toledo DSC Q100 module and Thermal Gravimetric Analysis (TGA) on a Mettler Toledo TGA Q5000 module. The sample size was ranging from 2 to 5 mg for DSC and 5 to 10 mg for TGA. Samples were placed in sealed pin-pricked aluminium pans for DSC experiments and alumina pans for TGA experiments. A heating rate of 10 °C min^{-1} in the

temperature range 30-300 °C was applied for DSC and TGA both. Samples were purged by a stream of dry nitrogen flowing at 80 mL min^{-1} for DSC and 50 mL min^{-1} for TGA.

4.4. Computational analysis. The experimental crystal structures were fully relaxed (including both the atomic positions and the lattice constants) with periodic density functional theory using the B86bPBE generalized gradient approximation (GGA) density functional (Becke86,PBE) and the exchange-hole dipole moment (XDM) dispersion correction.[54] All DFT calculations were performed using QuantumEspresso v6.4.1,[55] employing a 50 Ry planewave cutoff, a 500 Ry charge density cutoff, and 3x3x3 Monkhorst-Pack k-point grids (3x3x1 for form III). Core electrons were treated via the projector augmented wave (PAW) approach using PAW potentials for H, C, N, O, F, and S generated with Atomic v6.1.[55] The gas-phase B86bPBE-XDM calculations used in the conformational energy correction employed periodic boundary conditions with 20 Angstroms vacuum spacing separating periodic image molecules in each direction.[43]

The DLPNO-CCSD(T) calculations were performed in the aug-cc-pVTZ basis set using Orca v4.2.1.[56] Tight settings for both the self-consistent field calculation and the pair natural orbital selections were used to improve the fidelity of the approximation to canonical CCSD(T). The non-iterative (T0) triples DLPNO-CCSD(T) approximation[57] was used; test calculations in the smaller aug-cc-pVDZ basis set found that use of the iterative (T1) triples approximation[58] altered the relative polymorph energies by less than 0.2 kJ/mol. Complete-basis set (CBS)-limit DLPNO-CCSD(T) results were estimated[59] by combining the DLPNO-CCSD(T)/aug-cc-pVTZ results with CBS-limit second-order Møller-Plesset perturbation theory (MP2) energies that were computed with PSI4 v1.3.[60]

$$E_{CBS}^{DLPNO-CCSD(T)} = E_{CBS}^{MP2} + \left(E_{aug-cc-pVTZ}^{DLPNO-CCSD(T)} - E_{aug-cc-pVTZ}^{MP2} \right)$$

MP2 correlation energies were extrapolated to the complete basis set limit[61] using aug-cc-pVTZ and aug-cc-pVQZ results and then combined with aug-cc-pVQZ-level Hartree-Fock energies.

AUTHOR INFORMATION

Corresponding Author
*E-mail: sunilbhu28@gail.com, ashwini.nangia@gmail.com

ORCID
Sunil K. Rai: 0000-0001-5509-3142
Ashwini K. Nangia: 0000-0003-2442-7255
Anilkumar Gunnam: 0000-0003-4833-2314
Gregory J. O. Beran: 0000-0002-2229-2580
James A. Kaduk: 0000-0001-6610-541X

ASSOCIATED CONTENT

Supporting Information

List of screened solvents, crystallographic parameters, ORTEP diagrams, geometrical parameters of potential intra- and intermolecular interactions, structure determination from

PXRD, structure determination of form Ia from PXRD water content determination of peroxosolvate from ^{31}P NMR, and DSC and TGA thermogram can be obtained.

ACKNOWLEDGMENTS

SKR thanks SERB, New Delhi, India for the financial support (N-PDF fellowship 2016/001632) and CSIR-NCL, Pune, India for providing the infrastructure to carry out this work. Tata Institute of Fundamental Research, Hyderabad, India is acknowledged for ^{31}P NMR data acquisition. AKN thanks financial and infrastructure support from the University Grants Commission, New Delhi (through the UPE, CAS and IOE programs, Ministry of Education) and the Department of Science and Technology, New Delhi (through PURSE and FIST programs), and JC Bose Fellowship scheme of SERB (SR/S2/JCB-06/2009). G.B. gratefully acknowledges funding for this work from the U.S. National Science Foundation (CHE-1955554) and supercomputer time from XSEDE (TG-CHE110064).

References

1. Brittain, H. G. Polymorphism and solvatomorphism 2010. *J. Pharm. Sci.* **2012**, *101*, 464-484.

2. Lee, A. Y.; Erdemir, D.; Myerson, A. S. Crystal polymorphism in chemical process development. *Annu Rev Chem Biomol Eng* **2011**, *2*, 259-280.

3. Newman, A.; Wenslow, R. Solid form changes during drug development: good, bad, and ugly case studies. *AAPS Open*, **2016**, *2*, 1-11.

4. Bingham, A. L.; Hughes, D. S.; Hursthouse, M. B.; Lancaster, R. W.; Tavener, S.; Threlfall, T. L. Over one hundred solvates of sulfathiazole *Chem. Commun.* **2001**, 603–604

5. Campeta, A. M.; Chekal, B. P.; Abramov, Y. A.; Meenan, P. A.; Henson, M. J.; Shi, B., Singer, R. A.; Horspool, K. R. Development of a targeted polymorph screening approach for a complex polymorphic and highly solvating API. *J. Pharm. Sci.* **2010**, *99*, 3874-3886.

6. Boothroyd, S.; Kerridge, A.; Broo, A.; Buttar, D.; Anwar, J. Why do some molecules form hydrates or solvates? *Cryst. Growth Des.* **2018**, *18*, 1903−1908.

7. Hilfiker, R. Polymorphism: In the Pharmaceutical Industry; Hilfiker, R., Ed.; Wiley-VCH: Weinheim, FRG, 2006.

8. Cruz-Cabeza, A. J.; Reutzel-Edens, S. M.; Bernstein, J. Facts and fictions about polymorphism. *Chem. Soc. Rev.* **2015**, *44*, 8619-8635.

9. Guerain, M. A review on high pressure experiments for study of crystallographic behavior and polymorphism of pharmaceutical materials. *J. Pharm. Sci.* **2020**, *109*, 2640-2653.

10. Liu, Z.; Zhong, L.; Ying, P.; Feng, Z.; Li, C. Crystallization of metastable β glycine from gas phase via the sublimation of α or γ form in vacuum. *Biophys. Chem.* **2008**, *132*, 18-22.

11. Nath, N. K.; Aggarwal, H.; Nangia, A. Crystal Structure of Methyl Paraben Polymorph II. *Cryst. Growth Des.* **2011**, *11*, 967-971.

12. Braun, D. E.; Gelbrich, T.; Wurst, K.; Griesser, U. J. Computational and Experimental Characterization of Five Crystal Forms of Thymine: Packing Polymorphism, Polytypism/Disorder, and Stoichiometric 0.8-Hydrate. *Cryst. Growth Des.* **2016**, *16*, 3480-3496.

13. Solomos, M. A.; Capacci-Daniel, C.; Rubinson, J. F.; Swift, J. A. Polymorph Selection via Sublimation onto Siloxane Templates. *Cryst. Growth Des.* **2018**, *18*, 6965-6972.

14. Hua, C. T.; Shtukenberg, A. G.; Tan, M.; Vogt-Maranto, L.; Chan, E. J., Xu, W.; Yang, J.; Tuckerman, M. E.; Kahra, B. Discovering New Polymorphs of Paracetamol via Melt Crystallization. *Acta Cryst.* **2019**, *A75*, a328.
15. Li, X.; Ou, X.; Wang, B.; Rong, H.; Wang, B.; Chang, C.; Shi, B.; Yu, L.; Lu, M. Rich polymorphism in nicotinamide revealed by melt crystallization and crystal structure prediction. *Commun Chem* **2020**, *3*, 152.
16. Singh, A.; Lee, I. S.; Kim, K.; Myerson, A. S. Crystal growth on self-assembled monolayers. *CrystEngComm* **2011**, *13*, 24-32.
17. Diao, Y.; Harada, T.; Myerson, A. S.; Hatton, T. A.; Trout, B. L. The role of nanopore shape in surface-induced crystallization. *Nat. Mater.* **2011**, *10*, 867-871.
18. Meldrum, F. C.; O'Shaughnessy, C. Crystallization in confinement. *Adv. Mater.* **2020**, *32*, 2001068.
19. Lopez-Mejías, V.; Kampf, J. W.; Matzger, A. J. Nonamorphismin Flufenamic Acid and a New Record for a Polymorphic Compound with Solved Structures. *J. Am. Chem. Soc.* **2012**, *134*, 9872−9875.
20. Bhardwaj, R. M.; McMahon, J. A.; Nyman, J.; Price, L. S.; Konar, S.; Oswald, I. D. H.; Pulham, C. R.; Price, S. L.; Reutzel-Edens, S. M. A Prolific Solvate Former, Galunisertib, under the Pressure of Crystal Structure Prediction, Produces Ten Diverse Polymorphs. *J. Am. Chem. Soc.* **2019**, *141*, 13887−13897.
21. Liu, Y.; Gabriele, B.; Davey, R. J.; Cruz-Cabeza, A. J. Concerning Elusive Crystal Forms: The Case of Paracetamol. *J. Am. Chem. Soc.* **2020**, *142*, 6682–6689.
22. Levesque, A.; Maris, T.; Wuest, J. D. ROY Reclaims Its Crown: New Ways to Increase Polymorphic Diversity. *J. Am. Chem. Soc.* **2020**, *142*, 11873−11883.
23. Taylor, C. R.; Mulvee, M. T.; Perenyi, D. S.; Probert, M. R.; Day, G. M.; Steed, J. W. Minimizing polymorphic risk through cooperative computational and experimental exploration. *J. Am. Chem. Soc.* **2020**, 142, 39, 16668–16680.
24. Zeidan, T. A.; Trotta, J. T.; Tilak, P. A.; Oliveira, M. A.; Chiarella, R. A.; Foxman, B. M.; Almarsson, Ö.; Hickey, M. B. An Unprecedented Case of Dodecamorphism: The Twelfth Polymorph of Aripiprazole Formed by Seeding with Its Active Metabolite. *CrystEngComm* **2016**, *18*, 1486−1488.
25. Reutzel-Edens, S. M.; Bhardwaj, R. M. Crystal forms in pharmaceutical applications: olanzapine, a gift to crystal chemistry that keeps on giving. *IUCrJ* **2020**, *7*, 955–964.
26. Li, X.; Ou, X.; Rong, H.; Huang, S.; Nyman, J.; Yu, L.; Lu, M. The Twelfth Solved Structure of ROY: Single Crystals of Y04 Grown from Melt Microdroplets. *Cryst. Growth Des.* **2020**, *20*, 7093−7097.
27. Hodgkinson, P. NMR crystallography of molecular organics. *Prog. Nucl. Magn. Reson. Spectrosc.* **2020**, *118-119*, 10−53.
28. Broadhurst, E. T.; Xu, H.; Clabbers, M. T.; Lightowler, M.; Nudelman, F.; Zou, X.; Parsons, S. Polymorph evolution during crystal growth studied by 3D electron diffraction. *IUCrJ* **2020**, *7*, 5-9.
29. Haleblian, J.; McCrone, W. Pharmaceutical Applications of Polymorphism. *J. Pharm. Sci.* **1969**, *58*, 911-929.
30. Rai, S. K.; Gunnam, A.; Mannava, M. K. C.; Nangia, A. K. Improving the Dissolution Rate of the Anticancer Drug Dabrafenib. *Cryst. Growth Des.* **2020**, *20*, 1035–1046.

31. Desiraju, G. R. Supramolecular synthons in crystal engineering—a new organic synthesis. *Angew. Chem. Int. Ed.* **1995**, *34*(21), 2311-2327.
32. Almarsson, Ö.; Zaworotko, M. J. Crystal engineering of the composition of pharmaceutical phases. Do pharmaceutical co-crystals represent a new path to improved medicines?. *ChemComm* **2004**, *17*, 1889-1896.
33. Etter, M. C.; MacDonald, J. C.; Bernstein, J. Graph-set analysis of hydrogen-bond patterns in organic crystals. *Acta. Crystallogr. B. Struct. Sci. Cryst. Eng. Mater.* **1990**, *46*(2), 256-262.
34. Cole, J. C.; Taylor, R. Intermolecular Interactions of Organic Fluorine Seen in Perspective. *Cryst. Growth Des.* **2022**, *22*(2), 1352-1364.
35. Taylor, R. Which intermolecular interactions have a significant influence on crystal packing? *CrystEngComm* **2014**, *16*(30), 6852-6865.
36. Chopra, D.; Row, T. N. G. Role of organic fluorine in crystal engineering. *CrystEngComm* **2011**, *13*(7), 2175-2186.
37. Chopra, D.; Row, T. G. Evaluation of the interchangeability of C–H and C–F groups: insights from crystal packing in a series of isomeric fluorinated benzanilides. *CrystEngComm* **2008**, *10*(1), 54-67.
38. Hasija, A.; Bhowal, R.; Chopra, D. Quantitative Investigation of Weak Intermolecular Interactions of −F and $-CF_3$ Substituted in Situ Cryocrystallized Benzaldehydes. *Cryst. Growth Des.* **2020**, *20(12)*, 7921-7933.
39. Dikundwar, A. G.; Venkateswarlu, C.; Chandrakala, R. N.; Chandrasekaran, S.; Row, T. N. G. H/F isosteric substitution to attest different equi-energetic molecular conformations in crystals. *CrystEngComm* **2013**, *15*, 5403-5406.
40. Meanwell, N. A. Fluorine and Fluorinated Motifs in the Design and Application of Bioisosteres for Drug Design. *J. Med. Chem.* **2018**, *61*, 5822−5880.
41. Cruz-Cabeza, A. J.; Feeder, N.; Davey, R. J. Open questions in organic crystal polymorphism, *Commun. Chem.*, **2020**, 142.
42. Griesser, U. J.; Burger, A.; Mereiter, K. The polymorphic drug substances of the European Pharmacopoeia. Part 9. Physicochemical properties and crystal structure of acetazolamide crystal forms. *J. Pharm. Sci.* **1997**, *86*, 352-358.
43. Greenwell, C.; Beran, G. J. Inaccurate conformational energies still hinder crystal structure prediction in flexible organic molecules. *Cryst. Growth Des.* **2020**, *20*, 4875-4881.
44. Neese, F.; Wennmohs, F.; Hansen, A.; Becker, U. Efficient, approximate and parallel Hartree–Fock and hybrid DFT calculations. A 'chain-of-spheres' algorithm for the Hartree–Fock exchange. *Chem. Phys.* **2009**, *356*, 98-109.
45. Greenwell, C.; Beran, G. J. Rubrene untwisted: common density functional theory calculations overestimate its deviant tendencies. *J. Mater. Chem. C.* **2021**, *9*, 2848-2857.
46. Beran, G. J. Solid state photodimerization of 9-tert-butyl anthracene ester produces an exceptionally metastable polymorph according to first-principles calculations. *CrystEngComm* **2019**, *21*(4), 758-764.
47. Stahly, G. P. Diversity in Single- and Multiple-Component Crystals. The Search for and Prevalence of Polymorphs and Cocrystals. *Cryst. Growth Des.* **2007**, *7*, 1007−1026.

48. Kersten, K. M.; Breen, M. E.; Mapp, A. K.; Matzger, A. J. Pharmaceutical solvate formation for the incorporation of the antimicrobial agent hydrogen peroxide. *Chem. Commun.* **2018**, *54*, 9286-9289.
49. Chernyshov, I. Y.; Vener, M. V.; Prikhodchenko, P. V.; Medvedev, A. G.; Lev, O.; Churakov, A. V. Peroxosolvates: Formation Criteria, H_2O_2 Hydrogen Bonding, and Isomorphism with the Corresponding Hydrates *Cryst. Growth Des.* **2017**, *17*, 214–220.
50. APEX3, SAINT and SADABS; Bruker AXS Inc.: Madison, Wisconsin, USA, 2016.
51. Sheldrick, G. M. Crystal Structure Refinement with SHELXL. *Acta Crystallogr., Sect. C: Struct. Chem.* **2015**, 71, 3-8.
52. Farrugia, L. J. WinGX and ORTEP for Windows: an update. *J. Appl. Crystallogr.* **2012**, *45*, 849-854.
53. Spek, A. L. Structure Validation in Chemical Crystallography. *Acta Crystallogr., Sect. D: Biol. Crystallogr.* **2009**, *D65*, 148-155.
54. Otero-De-La-Roza, A.; Johnson, E. R. Van der Waals interactions in solids using the exchange-hole dipole moment model. *J. Chem. Phys.* **2012**, *136*, 174109.
55. Giannozzi, P.; Baroni, S.; Bonini, N.; Calandra, M.; Car, R.; Cavazzoni, C.; Ceresoli, D.; Chiarotti, G. L.; Cococcioni, M.; Dabo, I.; Corso, A. D.; de Gironcoli, S.; Fabris, S.; Fratesi, G.; Gebauer, R.; Gerstmann, U.; Gougoussis, C.; Kokalj, A.; Lazzeri,; Martin-Samos, L.; Marzari, N.; Mauri, F.; Mazzarello, R.; Paolini, S.; Pasquarello, A.; Paulatto, L.; Sbraccia, C.; Scandolo1, S.; Sclauzero, G.; Seitsonen, A. P.; Smogunov, A.; Umari, P.; Wentzcovitch, R. M. QUANTUM ESPRESSO: a modular and open-source software project for quantum simulations of materials. *J. Phys.: Condens. Matter* **2009**, *21*, 395502.
56. Neese, F. ORCA - an ab initio, Density Functional and Semiempirical Program Package, Version 2.4, Max-Planck Institut für Bioanorganische Chemie, Mülheim an der Ruhr, Germany, 2004.
57. Neese, F.; Wennmohs, F.; Hansen, A.; Becker, U. Efficient, approximate and parallel Hartree–Fock and hybrid DFT calculations. A ‘chain-of-spheres’ algorithm for the Hartree–Fock exchange. *Chem. Phys.* **2009**, *356*, 98-109.
58. Guo, Y.; Riplinger, C.; Becker, U.; Liakos, D. G.; Minenkov, Y.; Cavallo, L.; Neese, F. Communication: An improved linear scaling perturbative triples correction for the domain based local pair-natural orbital based singles and doubles coupled cluster method [DLPNO-CCSD (T)]. *J. Chem. Phys.* ***2018***, 148, 011101.
59. Otero-de-la-Roza, A.; Johnson, E. R. Van der Waals interactions in solids using the exchange-hole dipole moment model. *J. Chem. Phys.* **2012**, *136*, 174109.
60. Parrish, R. M.; Burns, L. A.; Smith, D. G. A.; Simmonett, A. C.; DePrince, A. E.; Hohenstein, E. G.; Bozkaya, U.; Sokolov, A. Y.; Di Remigio, R.; Richard, R. M.; Gonthier, J. F.; James, A. M.; McAlexander, H. R.; Kumar, A.; Saitow, M.; Wang, X.; Pritchard, B. P.; Prakash, V.; Schaefer, H. F., III; Patkowski, K.; Patkowski, K. Psi4 1.1: An Open-Source Electronic Structure Program Emphasizing Automation, Advanced Libraries, and Interoperability. *J. Chem. Theory Comput.* **2017**, *13*, 3185−3197.
61. Feller, D. Application of systematic sequences of wave functions to the water dimer. *J. Chem. Phys.* **1992**, *96*, 6104-6114.

Polymorphs, Solvatomorphs, Hydrate and Perhydrate of Dabrafenib

Sunil K. Rai,*[a,c] Anilkumar Gunnam,[b] Gregory J. O. Beran,[d] James A. Kaduk,[e] and Ashwini K. Nangia*[b,c]

[a] Department of Chemistry, Faculty of Science, University of Lucknow, Lucknow, Uttar Pradesh 226007, India
[b] School of Chemistry, University of Hyderabad, Prof. C. R. Rao Road, Gachibowli, Central University P.O., Hyderabad 500 046, India
[c] Division of Organic Chemistry, CSIR − National Chemical Laboratory, Dr. Homi Bhabha Road, Pune 411008, India
[d] Department of Chemistry, University of California Riverside, Riverside CA 92521, USA.
[e] Illinois Institute of Technology, 3101 S. Dearborn St., Chicago, Illinois 60616, USA and North Central College, 131 S. Loomis St., Naperville, Illinois 60540, USA

TOC

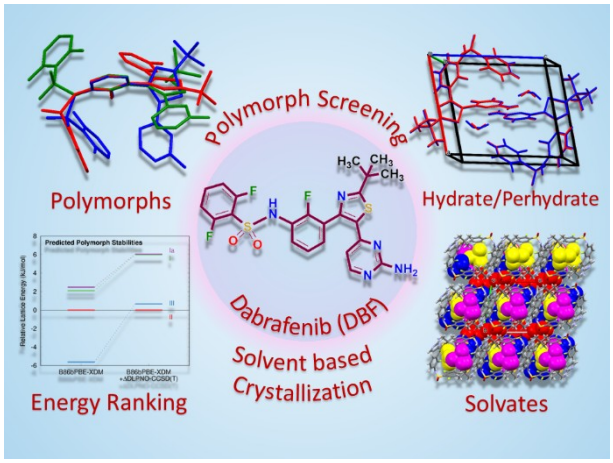

An extensive crystal form screening of the anticancer drug Dabrafenib (DBF) produced three crystal forms (I, II and III) of the drug, a monohydrate, an isomorphous peroxo solvate, and eight different solvates with ethyl acetate, dichloromethane, chloroform, carbon tetrachloride, 1,1,2,2-tetrachloroethane, tetrachloroethylene, benzene, and anisole of DBF. The relative stability of the drug polymorphs was calculated using B86bPBE-XDM+ΔDLPNO-CCSD(T) function which showed that form II is the most stable polymorph and, form III and form I are progressively less stable. The isomorphous peroxo solvate showed ~9.5% of residual water occupancy quantified by ^{31}P NMR analysis using triphenylphosphine oxide chemical reaction. With its high molecular flexibility, a prolific solvate potential and drug polymorphism, the present work opens opportunity for further solid form landscape study of the popular anticancer drug Dabrafenib.